ELSEVIER

Journal of Materials Processing Technology 136 (2003) 190–201

Journal of Materials Processing Technology

www.elsevier.com/locate/jmatprotec

An evaluation of gas quenching of steel rings by multiple-jet impingement

Jérôme Ferrari[a], Noam Lior[b,*], Jan Slycke[c]

[a]*Faxén Laboratory, Royal Institute of Technology, S-100 44 Stockholm, Sweden*
[b]*Department of Mechanical Engineering and Applied Mechanics, University of Pennsylvania, 297 Towne Building, 220 South 33rd Street, Philadelphia, PA 19104-6316, USA*
[c]*SKF Engineering and Research Centre BV, NL-3430 DT Nieuwegein, The Netherlands*

Received 7 June 2002; received in revised form 7 June 2002; accepted 14 January 2003

Abstract

Multiple gas jet impingement cooling for quenching is a very promising approach for increasing the heat transfer coefficients (h) and thus the overall cooling rates in the gas-quenching process. Appropriate correlations for h were selected based on an extensive critical literature review, and used in a numerical heat conduction model and a numerical phase transformation model which were developed and solved for evaluating the quenching capacity of such cooling methods for quenching steel rings. The models allow prediction of the steel phase transformation extent as a function of h, for different ring sizes. An optimization of the jet nozzle dimensions and configuration was performed, and the effects of the jet spent flow and the cooling gas temperature were discussed and estimated. It was also found that while the spent flow effect on h is not adequately known, it tends to lower h, while the cooling gas temperature has minimal effect on h. Validation experiments were performed and show that the predicted trends are reasonable, within the errors of the Johnson–Mehl–Avrami phase transformation model and the experimental method used.

Keywords: Quenching; Gas quenching; Impingement cooling; Phase transformations

1. Introduction

The use of gas instead of liquid as quenchant has environmental, product quality, process control, safety and economic advantages (cf. [1]) and its improvement is under intensive study at the Faxén Laboratory of the Royal Institute of Technology, Sweden (cf. [2–4]). The primary effort is focused on finding ways to generate sufficiently high heat transfer coefficients, and to produce cooling which results in minimal distortions of the quenched parts. Due to the high heat transfer coefficients it produces, jet impingement, which is increasingly used in industry to cool, heat or dry a surface in applications such as cooling of gas turbine components, drying of textile, film and paper, and annealing of metal and plastic sheets, is of interest here. It has been the topic of many papers and several reviews; the most relevant ones to this study being those by Martin [5] and Viskanta [6].

While impinging multi-jet quenching has appeared in a commercial quenching device, no basic studies of its thermal and metallurgical effects have been found in the literature. The commercial product was intended for use in the bearing industry for air-quenching of ring-shaped products. Such products are often manufactured in a through hardening bearing steel like the 52100 steel (ASTM A295-98 52100), which has limited hardenability, that is, for a given quenching intensity, non-martensitic transformation products tends to form in thicker wall sections.

This study aims at identifying the parameters controlling the heat transfer in multi-jet impingement gas quenching so that the process could be optimized. To propose some improvements in the design to increase the heat transfer coefficient, a literature study on multiple impinging jets has been made. To evaluate the effect of the heat transfer coefficients on the properties of the ring, a numerical model of the heat conduction inside the ring has been developed using FEMLAB® [7] and a phase transformation one using MATLAB® [8]. An annular nozzle-field gas-quenching device will be considered, and the results of the investigations will be displayed.

* Corresponding author. Tel.: +1-215-898-4803; fax: +1-215-573-6334.
E-mail address: lior@seas.upenn.edu (N. Lior).

0924-0136/03/$ – see front matter © 2003 Elsevier Science B.V. All rights reserved.
doi:10.1016/S0924-0136(03)00158-4

Nomenclature

A	area of the heat exchanging surface (m^2)
b	temperature dependent parameter in Section 4.3
C_p	heat capacity (J/kg K)
d	jet diameter (m)
f	relative nozzle area, Eqs. (1)–(3)
h	heat transfer coefficient ($W/m^2/K$)
H	jet to plate distance (m)
k	thermal conductivity (W/m K)
l	ring wall thickness (m)
L	ring height (m)
n	temperature dependent parameter in Section 4.3
Δp	pressure drop (Pa)
P	power of the blower (W)
Pr	Prandtl number $= C_{pg}\mu_g/k_g$
r	inner radius of the ring (m)
Re	Reynolds number $= \rho_g w d/\mu_g$
t	jet pitch, m (or time, s)
$t_{0.01}$	time needed to reach a transformed phase fraction of 0.01 at constant temperature (read from a TTT-diagram) (s)
$t_{0.99}$	time needed to reach a transformed phase fraction of 0.99 at constant temperature (read from a TTT-diagram) (s)
T	temperature (K)
ΔT	temperature difference between the gas and the ring surface (K)
T_g	gas temperature (K)
T_I	initial temperature (i.e. at quenching start) (K)
V	volumetric flow rate (m^3/s)
V_a	flow rate by array of jets (m^3/s)
w	nozzle exit velocity (m/s)
w_c	crossflow (gas flowing perpendicularly to the jets) velocity (m/s)
X	jet pitch in the direction of the crossflow (m)
Y	jet pitch in the direction perpendicular to the crossflow (m)
z	fraction of transformed phase (pearlite or bainite)

Greek letters

μ	dynamic viscosity (Pa s)
ξ	pressure loss coefficient
ρ	density (kg/m^3)

Subscripts

av	average
g	gas
m	metal

2. Description of the nozzle-field gas-quenching device

A commercial nozzle-field gas-quenching system is presented in a simplified way in Fig. 1. After austenitization, the rings are placed one at a time in the device for quenching.

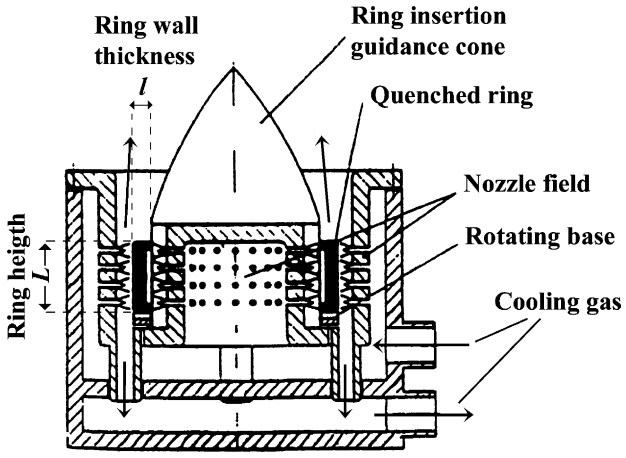

Fig. 1. The nozzle-field gas-quenching device for rings.

The air (or nitrogen) at approximately atmospheric pressure is blown into the device. The air passes at high speed through the inner and the outer nozzle fields and impinges on the inner and outer faces of the rings. It then exits the device in the upward and downward directions. The ring lies on a rotating base, which makes it spin, improving the uniformity of the cooling. The gas jets formed in this way generate high heat transfer rates between the ring and the air.

In the original design $t = 5$ mm, $d = 1$ mm and $H = 5$ mm. If we assume an air jet velocity of 100 m/s and 1 bar at the exit, the jet Reynolds number, Re, is about 7000.

3. Prediction of the heat transfer coefficient

A variety of formulas, empirical and semi-empirical, for the convective heat transfer coefficient produced by arrays of nozzles impinging on a flat plate are found in the literature. The sources of the most suitable ones, their range of validity, the differences in the values of h that they predict (based on the base-case nozzle arrangement $H = 5$ mm, $t = 5$ mm, $d = 1$ mm, and jet velocity of 100 m/s) are summarized in Table 1. The formulas and their evaluation are described in detail in [9].

It can be seen from Table 1 that (a) the Gromoll's [14] formula predicts the highest values of h and is thus the most optimistic one, and (b) the different formulas predict widely varying values of h, with the highest being 79% larger than the lowest. These discrepancies may be due the substantially different experimental setup used by the different authors.

While all the formulas were evaluated in this study, Martin's formula [5] was found to be most suitable. Gathering the work of several other authors, he used empirical data for single jet impingement heat transfer to develop an analytical equation for multiple (staggered or in-line) jets. This equation has shown good agreement with several sets of experimental data. He assumes that the flow from a jet is not disturbed by

Table 1
Comparison of the presented formulas. The values of h are calculated for $H = 5$ mm, $t = 5$ mm, $d = 1$ mm, and $w = 100$ m/s

Formula	*Re* range of validity	*t*/*d* (or *f*) range of validity	*H*/*d* range of validity	*h* (W/m^2/K)	Notes
Martin [5]	2×10^3 to 10^5	4×10^{-3} to 4×10^{-2}	2–12	787	Spent flow negligible
Ott [10]	6.7×10^3 to 1.57×10^4	6	3.75–15	764	Spent flow exits parallel to the jets
Glaser [11]	5×10^3 to 5×10^4	3–7.5	1–8	787	
Kercher and Tabakoff [12]	3×10^2 to 3×10^4	3.1–12.5	1–4.8	1125	
Gardon and Cobonpue [13]	10^3 to 10^5	4–32	8–127	1169	Long tubes
Gromoll [14]	1.21×10^4 to 2.47×10^4	3.33–37.5	0.08–18.75	1368	Conical tubes

the "spent flow" (the flow after the impingement) of the neighboring jets. It is probably the best available now since it has the widest range and is validated by many different experiments.

It is

$$h_{\mathrm{av}} = \frac{k_{\mathrm{g}}}{d}\left[1 + \left(\frac{H/d}{0.6}\sqrt{f}\right)^6\right]^{-0.05} \times \frac{\sqrt{f}(1 - 2.2\sqrt{f})}{1 + 0.2(H/d - 6)\sqrt{f}} Re^{2/3}\, Pr^{0.42} \quad (1)$$

where f is the relative nozzle area, given by the ratio of the nozzle exit cross-section to the area of the inline or the hexagon attached to it.

For inline arrays of jets

$$f = \frac{1}{4}\frac{\pi d^2}{t^2} \quad (2)$$

and for staggered arrays of jets

$$f = \frac{1}{6}\frac{\pi\sqrt{3}d^2}{t^2} \quad (3)$$

Range of validity

$$2000 \le Re \le 100\,000, \qquad 0.004 \le f \le 0.04$$

4. The heat conduction and phase transformation model

4.1. The approach

To quench the 52100 steel, it is first austenitized, which means that it is heated and kept at high temperature (about 860 °C) for a few minutes to guarantee a controlled partial dissolution of cementite in austenite. Then it is cooled quickly to allow a martensitic transformation. To produce a fully martensitic transformation, it is sufficient to ensure that no pearlite and no bainite had time to form before the martensitic temperature is reached (240 °C). The models presented here will thus only address the pearlitic and bainitic transformation, and it is assumed that the pearlitic and bainitic contents remain low, specifically, below 2% transformed phase (pearlite + bainite).

To estimate whether the convective heat transfer coefficients predicted by the formulas in Section 3 are sufficiently high to produce a fully martensitic transformation during quenching, two numerical models have been developed:

- A heat conduction model to compute the temperature field history in an austenitic body during quenching.
- A phase transformation model to estimate the phase transformation of austenite to pearlite and bainite occurring during quenching as a function of temperature.

Combining these models, computations were made for various steel ring sizes to determine the h needed to quench a ring for a certain transformation fraction.

4.2. The conduction model

Using the finite element unstructured-grid program FEMLAB® [7], a model was developed to simulate the cooling of a ring during multiple impinging jet quenching, to obtain cooling curves that would be used for predicting phase transformation behavior (in Section 4.3). This model solves the transient three-dimensional axisymmetric cylindrical-coordinate heat conduction equation:

$$\rho_{\mathrm{m}} C_{p_{\mathrm{m}}} \frac{\partial T}{\partial t} - \mathrm{div}(k_{\mathrm{m}} \cdot \mathrm{grad}(T)) = 0 \quad (4)$$

with the initial conditions $T_{\mathrm{I}} = 860$ °C, uniform in the ring. The boundary conditions are

$$-k_{\mathrm{m}} \cdot \mathrm{grad}(T) = h(T - T_{\mathrm{g}}) \quad (5)$$

where it is assumed that the air is blowing at the cylinder is at $T_{\mathrm{g}} = 20$ °C, and, because of the typically close spacing of the jets, that h on the outer and inner circumferential area is uniform. Based on Kübler [15], it is assumed that h on the upper and lower faces of the ring is 10% of the h on the inner and outer circumferential surfaces on which the jets impinge.

The ring is 52100 steel (austenite) having $k_{\mathrm{m}} = 15.0 + 0.0142\,T$ W/m K, $\rho_{\mathrm{m}} = 7810$ kg/m^3, $C_{p\mathrm{m}} = 635$ J/kg K.

As an example of the obtained solution, Fig. 2 shows the temperature field in the cross-section of a 6.3 mm thick ring after 10 s of cooling with $h = 848$ W/m^2/K on the inner

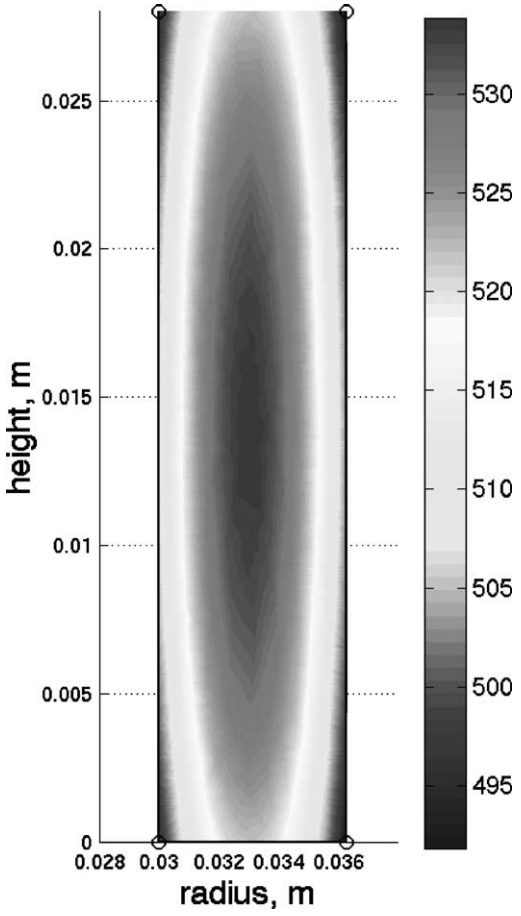

Fig. 2. The computed temperature field in the cross-section of a 6.3 mm thick ring with a 60 mm internal radius, after 10 s with $h = 848$ W/m^2/K applied on the inner (left) and outer (right) faces and a h of 84.8 W/m^2/K on the upper and lower faces. The color bar on the right gives the temperature scale in °C.

(left) and outer (right) cylindrical surfaces and $h = 84.8$ W/m^2/K on the upper and lower faces. One can see, for example, that the ring corners are about 45 °C colder than the center of its wall.

4.3. The phase transformation model

Transformation of austenite to pearlite and bainite are diffusion controlled solid-state reactions and as such they are of heterogeneous type, meaning that they rely on a nucleation and growth sequence. This is a complex process [16–21], but its overall progress can be well described as a thermally activated transformation. Thus, knowing the temperature history at every point in the quenched body, and the TTT-diagram corresponding to the steel studied, it is possible to compute the phase transformations occurring during the quenching process. This should allow determining whether given cooling rates computed as described in Section 4.2 would produce a microstructure free from diffusion controlled transformation products, that is, a microstructure consisting of martensite and retained austenite (and any cementite, not dissolved during the austenitization process).

Several models are available to describe the temperature and time dependent progress of the kinetics of various types of reactions. One frequently used model for solid-state reactions is the Avrami model (sometimes called the Johnson–Mehl–Avrami or JMA model) [17–20]. Although these equations have a foundation in the metal physics, they still are approximations of the reality and there is no generally valid theoretical justification for the JMA type equations [20]. For example, a solid-state reaction may consist of several subsequent stages (like nucleation and growth), which are difficult to resolve. Each of these stages will have its own reaction kinetics and may, for example, exhibit different activation energies. Furthermore, global transformation models like the Avrami model also incorporate the assumption that the material has a uniform composition and thereby uniform transformation properties throughout the material volume considered. Fluctuations in the composition always exist, however, due to such phenomena as macroscopic segregation, microscopic scale variations due to phenomena such as carbide dissolution, and consequent variations in transformation properties.

Using the Avrami equation to characterize the overall reaction means that the parameter values (like the activation energy) will get the character of "effective" parameters. The equations should therefore be seen as regression formulas, which usually give a good description of experimental information, but which should be used with caution for extrapolation outside the experimental range.

The phase transformation model outlined and used here is described in detail in Sjöström [22] and Thuvander [23]. According to Avrami [17–19], the fraction of a transformed phase, z (pearlite or bainite) formed after keeping the body for t seconds at a constant temperature T, is

$$z = 1 - \exp[-b(T)t^{n(T)}] \tag{6}$$

where b and n are two temperature dependent parameters. They can be deduced from Eq. (6) by knowing two of its solutions, for example, by using a TTT-diagram. Here, the TTT-diagram for 52100 steel, austenitized during 10 min at 860 °C, is used, see Fig. 3. After this austenitization treatment the microstructure consists of austenite containing partially undissolved cementite particles. The transformation start and finish curves from that TTT-diagram give the time needed to reach the fraction of 0.01 and 0.99 for each transformed phase ($t_{0.01}$ and $t_{0.99}$). Then, from Eq. (6), we obtain

$$n(T) = \frac{\ln[\ln(1-0.01)/\ln(1-0.99)]}{\ln[t_{0.01}(T)/t_{0.99}(T)]} \tag{7}$$

$$b(T) = -\frac{\ln(1-0.01)}{t_{0.01}(T)^{n(T)}} \tag{8}$$

Eq. (6) is only valid for a constant temperature process. To simulate the phase transformation occurring during the

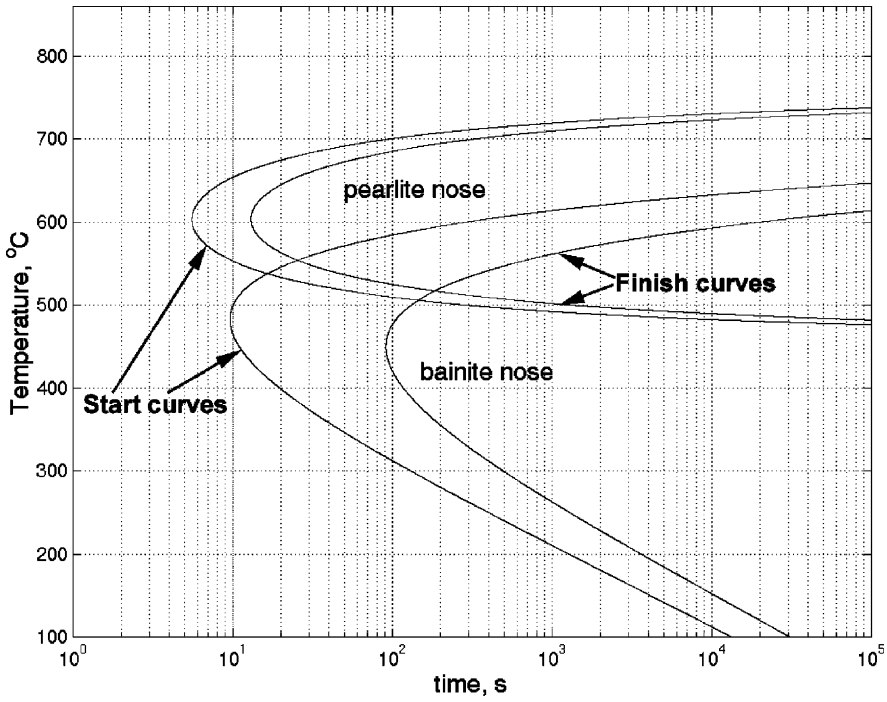

Fig. 3. The TTT-diagram used for the computation, suitable for 52100 steel austenitized during 10 min at 860 °C. Extrapolated from the SKF Steel Black Book, 1982.

varying temperature process, it is approximated here as a succession of small constant temperature time-steps, during each of which a constant temperature transformation occurs. The final fraction of transformed phase is regarded as the sum of all the small fractions formed at each time-step. To compute the fraction created at a specific time-step, we need to calculate the fraction formed at the temperature T during that time-step, knowing the fraction z already formed at the beginning of the time-step. The differentiation of Eq. (6) yields the transformation rate as

$$\frac{dz}{dt} = b(T)n(T)t^{n-1}\exp[-b(T)t^{n(T)}] \tag{9}$$

Thus in Eq. (9), t is not the time at which the fraction is created, but the fictitious time needed to get the current amount of transformed phase at the constant temperature T. From Eq. (6), we get

$$t = \left[\frac{-\ln(1-z)}{b(T)}\right]^{1/n(T)} \tag{10}$$

Combining (9) and (10) gives

$$\frac{dz}{dt} = b(T)n(T)\left[\frac{-\ln(1-z)}{b(T)}\right]^{(n(T)-1)/n(T)}(1-z) \tag{11}$$

Time integration of Eq. (11) gives the amount of phase transformed during quenching

$$\int_{\text{start}}^{\text{end}} b(T)n(T)\left[\frac{-\ln(1-z)}{b(T)}\right]^{(n(T)-1)/n(T)}(1-z)\,dt \tag{12}$$

Several additional qualifications of the popular Avrami [17–19] Eq. (6) used here are noteworthy at this point. It incorporates the assumption that the transformation starts immediately, while there is evidence [21] of the existence of an "incubation time", before the transformation starts. In their experiments with the SAE 1080 steel, Hawbolt et al. [21] found an incubation time, which was typically 80% of $t_{0.01}$. This may cause large discrepancies in the simulated results, especially at low transformed phase content, since the real transformation begins much later than modeled. For the 52100 steel, assuming an incubation time of 80% of $t_{0.01}$ and a constant temperature transformation process, the equation was found to have an error of at least 20% in the estimation of the time at which 0.1% transformed phase is created. An attempt to incorporate the "incubation time" concept in the simulation was made, but it was found that its successful completion would require much more research, and better transformation data.

4.4. The computations

Using the solutions of the heat conduction equations (4) and (5) for different values of h combined with the phase transformation equation (12), computations to find the convective heat transfer coefficient needed to reach 0.1, 0.3, 0.5, 1.0 and 2.0% of transformed (pearlite + bainite) phase were made for rings with rectangular wall cross-section, for wall thickness, l varying from 4 to 15 mm. The inner diameter and the width of the rings were, respectively, 10 and 2.2 times the ring wall thickness l.

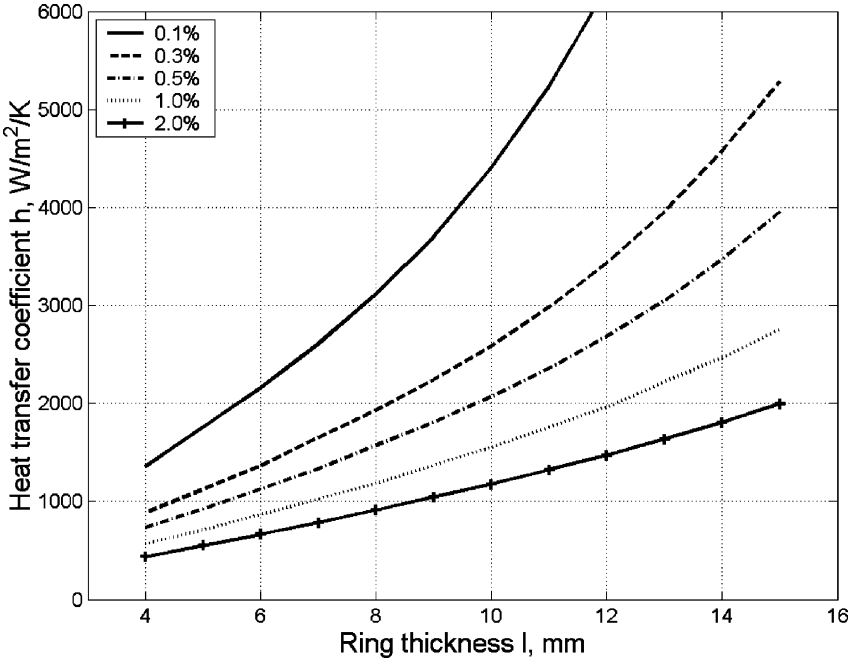

Fig. 4. The heat transfer coefficient h, needed to obtain a certain amount of transformed phase (pearlite + bainite), as a function of the ring thickness. The different curve lines indicates the amount of transformed phase. The 0.1% curve, truncated here for clearness reaches $h = 11\,861$ W/m^2/K for a ring thickness of 15 mm.

4.5. Results

The results of the computation are displayed in Figs. 4 and 5. The heat transfer coefficient h needed to quench a ring is predicted to increase exponentially with l, and obviously larger h are needed if smaller amounts of transformation products are desired.

The theoretical predictions are compared with experimental results for 6.3 mm thick rings in Fig. 5, austenitized as indicated in the figure caption, again producing an

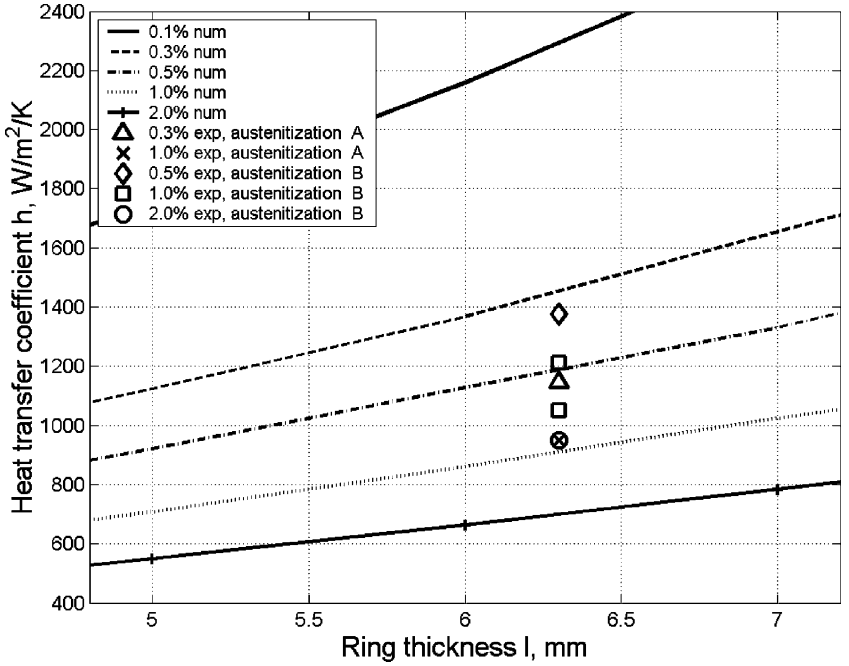

Fig. 5. The heat transfer coefficient, h, needed to obtain a certain amount of transformed phase (pearlite + bainite), as a function of the ring thickness. The curves represent the amount of transformed phase obtained from the numerical model, and the markers are the experimental results. The experiments were performed on SAE 52100 steel, for two different austenitizations at: (A) 860 °C during 26 min and (B) 905–910 °C during 14 min.

austenite containing partially undissolved cementite particles. During the experiments, rings were quenched in the device, and the heat transfer coefficient, h, was controlled by varying the blower output pressure. The pressure was measured, and related to the total gas flow rate by additional experiments. Knowing the total gas flow, the jet velocity was calculated by dividing it by the number of jets; assuming the same gas velocity in each jet. The gas velocity was incorporated in the Martin's [5] formula to compute h. The amount of transformed phase formed during the quench was determined afterwards by an expert, who used visual observation to estimate transformation values of 0.1, 0.3, 0.5, 1.0, 2.0%. High accuracy is therefore not expected, as also seen by the presence of the two different observations for the same conditions (the square marks in Fig. 5).

As shown in Fig. 5, the trends of the experimental data are correct, in that lower transformation percentages consistently require higher heat transfer coefficients, and the disagreement between the absolute values of the experiments and numerical analysis is rooted in uncertainties in (1) Martin's [5] formula for evaluating h, (2) value and uniformity of the velocity among the jets, (3) the experimental (manual/visual) method for measuring the amount of transformed phase, (4) the Avrami type models especially for very low fractions of transformation products, and (5) the available TTT-diagrams, which were found to show variation of $t_{0.01}$ and $t_{0.99}$ as large as 40% (cf. [21]). Obviously, this comparison should be revisited, by finding ways to minimize these problems.

5. Device configuration optimization

There are many parameters that can be changed to improve the heat transfer rates, and we have first addressed the spatial arrangement of nozzles. The objective function in the optimization was the convective heat transfer coefficient, which is sought to be maximized. Using Martin's [5] formula, configuration optimization was performed in two ways: (1) maintaining the blower power constant, and (2) maintaining the gas velocity constant. All the results presented below are found assuming that the spent flow has a negligible effect, and more discussion of this effect is given in Section 6.

5.1. Optimization assuming constant blower power, P

Martin's analysis [5] is based on the assumption of constant blower power, a sensible engineering approach. First, the nozzle exit velocity w has to be expressed as a function of the blower power P, which is calculated by

$$P = \Delta p V \tag{13}$$

where Δp is the overall pressure drop that the blower has to overcome in generating the nozzle flow, and which can be calculated from

$$\Delta p = \xi\left(\tfrac{1}{2}\rho_g\right)w^2 \tag{14}$$

where ξ is the pressure loss coefficient, the sum of all flow resistance between the blower and the nozzle exit, here assumed to be constant, and ρ_g is the gas density, also assumed to be constant.

The volumetric flow rate V can be calculated from

$$V = wfA \tag{15}$$

where f is the relative nozzle area Eqs. (1)–(3), and A is the area of the heat exchanging surface. Combining Eqs. (13)–(15), w can then be expressed as

$$w = \left(\frac{2P}{\xi\rho_g f A}\right)^{1/3} \tag{16}$$

By looking for the optimized arrangement, one will find that the reduction of all three characteristics lengths (d, H and t) results in a monotonically increasing heat transfer coefficient. As pointed out by Martin [5], a certain minimal distance H will often be imposed for practical reasons. It can then be calculated analytically [5], or numerically (with MATLAB®, [8]), that the maximal h is obtained for $d = 0.184\,H$, and $t = 1.423\,H$ for staggered arrays of nozzles, or $t = 1.324\,H$ for inline arrays of nozzles.

Figs. 6–8 show the variation of h with two characteristics lengths, while the other one is maintained constant. Fig. 9 shows the nozzle exit velocity varying with d and t for $H = 0.005$ m. Here we have chosen the values of P, Δp, and ξ to obtain $w = 100$ m/s in the original nozzle arrangement, which is a typical gas velocity in a nozzle-field gas-quenching device. The nozzle arrangement was assumed to be inline. The numbers written on the contour plots are in W/m^2/K for Figs. 6–8, and in m/s for Fig. 9. It can be seen from Figs. 6 and 8 that the heat transfer coefficient is not very sensitive to the jet diameter. From Figs. 7 and 8, it can be concluded that a small jet-to-plate distance H is preferable.

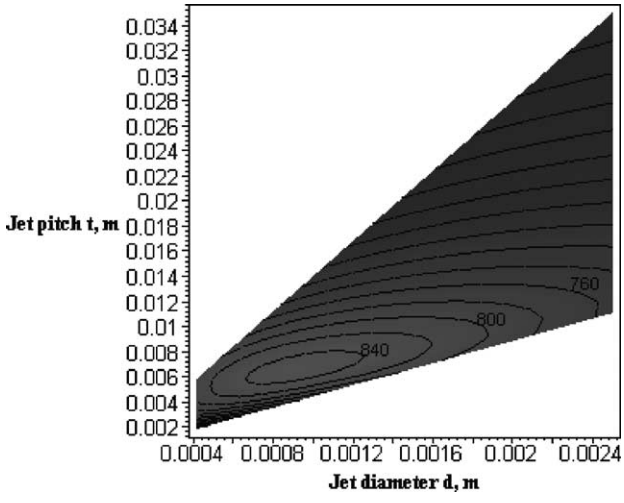

Fig. 6. Constant heat transfer coefficient, h contours in W/m^2/K, as a function of d and t for $H = 0.005$ m, inline jet arrangement and constant blower power.

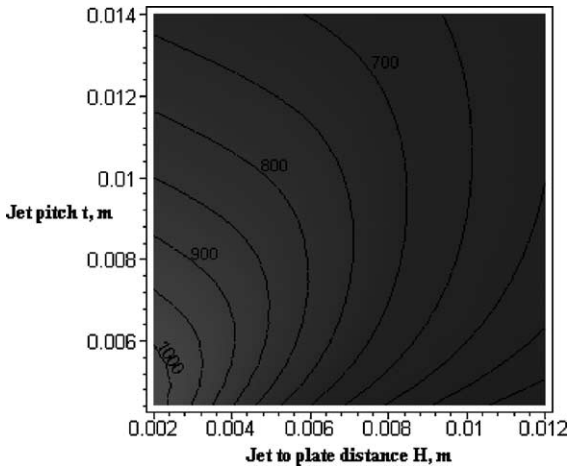

Fig. 7. Constant heat transfer coefficient, h contours in W/m^2/K, as a function of H and t for $d = 0.001$ m, inline jet arrangement and constant blower power.

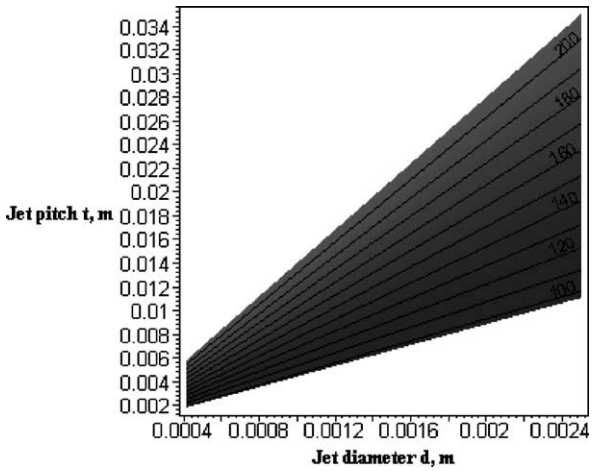

Fig. 9. Constant nozzle exit velocity, w contours in m/s, as a function of d and t for $H = 0.005$ m, inline jet arrangement and constant blower power.

5.2. Optimization assuming constant gas velocity, w

Here it is assumed that a desired gas velocity can be reached for any nozzle arrangement, and thus that the blower power is not constrained. This maximum attainable jet velocity w can reasonably be estimated as being equal to Mach 0.9 to avoid sonic velocities which result in excessive power consumption and choking. Knowing that $Re = \rho_g w d/\mu_g$, Eq. (1) can be rewritten as

$$h_{av} = f(H, t, d)w^{2/3} \tag{17}$$

Thus all the results below, which are established with $w = 100$ m/s can be easily rescaled for another velocity.

The presentation logic of Figs. 10–12 corresponds to that of Figs. 6–8. Fig. 13 shows the relative power consumption as a function of d and t for $H = 0.005$ m, an arbitrary reference power consumption magnitude of 1 is chosen for the original arrangement of $d = 0.001$ m, $t = 0.005$ m, $H = 0.005$ m.

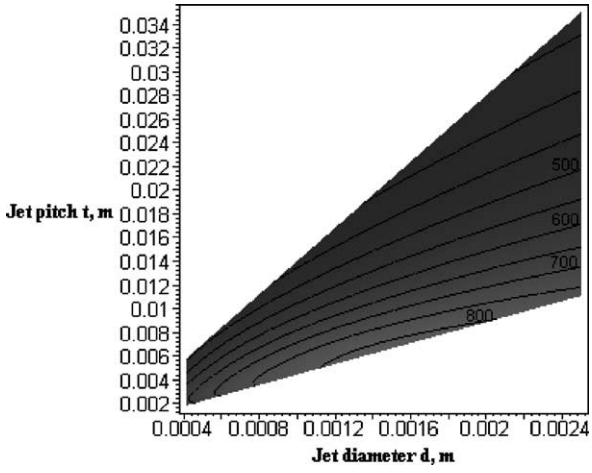

Fig. 10. Constant heat transfer coefficient, h contours in W/m^2/K, as a function of d and t for $H = 0.005$ m, inline jet arrangement and constant nozzle exit velocity.

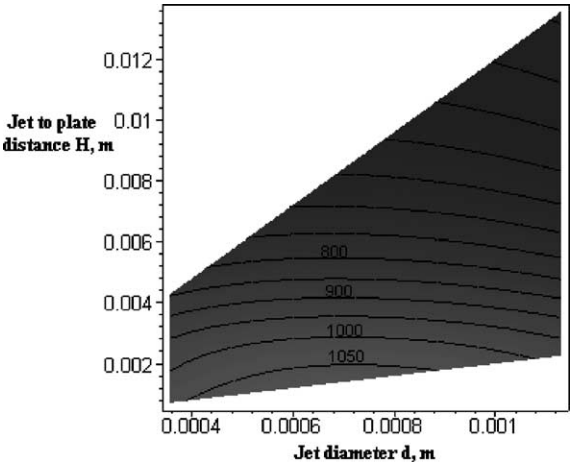

Fig. 8. Constant heat transfer coefficient, h contours in W/m^2/K, as a function of d and H for $t = 0.005$ m, inline jet arrangement and constant blower power.

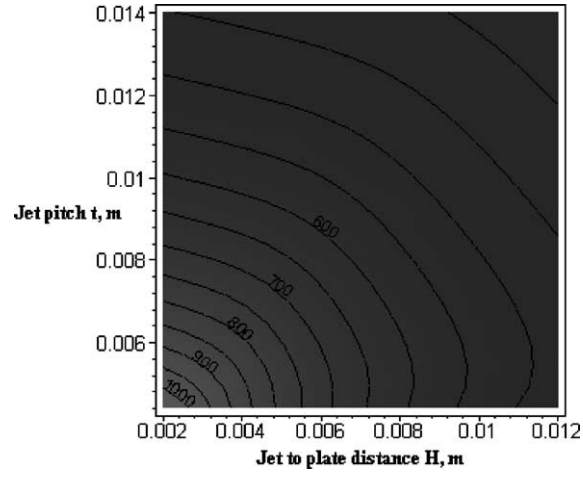

Fig. 11. Constant heat transfer coefficient, h contours in W/m^2/K, as a function of H and t for $d = 0.001$ m, inline jet arrangement and constant nozzle exit velocity.

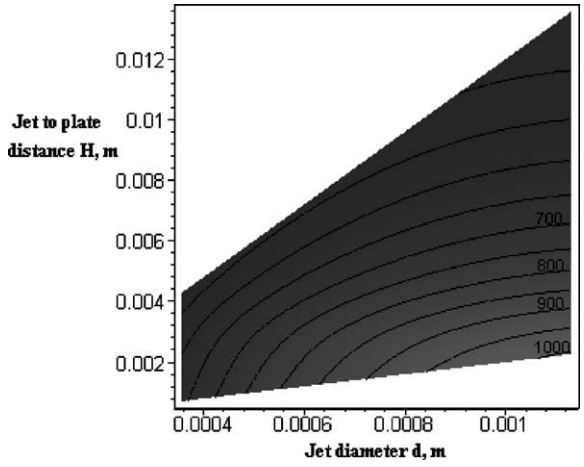

Fig. 12. Constant heat transfer coefficient, h contours in W/m^2/K, as a function of d and H for $t = 0.005$ m, inline jet arrangement and constant nozzle exit velocity.

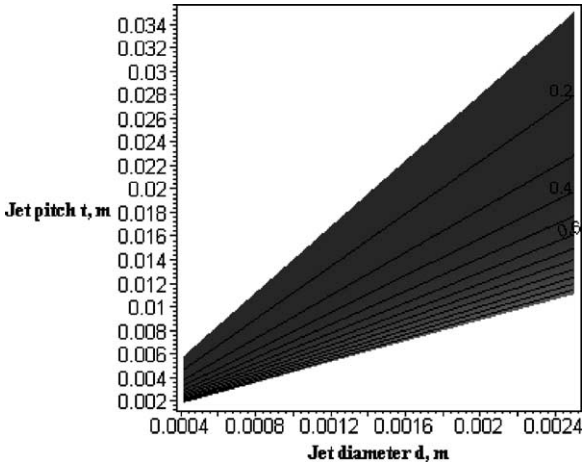

Fig. 13. Constant relative power consumption contours as a function of d and t for $H = 0.005$ m, inline jet arrangement and constant nozzle exit velocity. A power consumption of 1 is chosen for the original arrangement ($d = 0.001$ m, $t = 0.005$ m, $H = 0.005$ m).

The nozzle arrangement is again inline. It can be seen from these figures that there is no optimal arrangement of nozzles in the range of validity of Martin's [5] equation. Once again, the jet diameter d is the parameter with the least influence on h, noting at the same time that h does increase with d. It is clear from Figs. 11 and 12 that H should be minimized and from Figs. 10 and 11 that t also should be minimized, the latter meaning that the number of jets should be maximized. Briefly summarized, in this case where the blower power is unconstrained, as much air as possible should be blown at the ring, with the nozzles as close as possible to it.

6. The "spent flow"

Coming out from the nozzles, the air impinges on the ring and therefrom becomes part of the "spent flow". This "used" air forms a crossflow, flowing laterally between the jets to exit the cooling apparatus. Obviously, the spent flow affects the direction and velocity of the jets, and may thus affect their cooling capability. The presence of the spent flow represents a complex and important problem in multiple impinging jets cooling and, from all available evidence, its effect should not be neglected. In fact, the Kercher and Tabakoff [12] formula suggests a 12% reduction of the local heat transfer coefficient due to the spent flow, but definitive general information on this effect is unavailable and was thus not included in the analysis. Interpretation of the results should thus be done carefully. While its influence is still not fully understood, some characteristics are explained below in the context of attempting to reduce any cooling rate reductions it may cause.

In the nozzle-field gas-quenching device (Fig. 1), the spent flow escapes upwards and downwards, parallel to the axis of the ring. As it moves toward the exits, the spent flow quantity increases, being fed by the successive spent jets it meets. Thus, the spent flow strength depends highly on the ring height. If the air in the nozzle-field gas-quenching device escapes symmetrically upwards and downwards, then the spent flow has its maximal effect on heat transfer at the ring edges, and literally no effect in the symmetric axial midplane. It consequently results in a higher heat transfer coefficient at the ring center than at the edges.

Florschuetz et al. [24] conducted a large set of experiments and some analysis to understand the effect of the spent flow. They developed an equation for assessing this effect, but it is only valid for jet-to-plate distances ranging from 1 to 3 jet diameters, d, which is too small to be useful in the present case. An attempt to associate this equation with Martin's [5] formula did not give any consistent result. In general, the experiments of [24] pointed out that choosing an inline arrangement of nozzles instead of a staggered one can improve h by up to 40% when the spent flow effects are considered. The explanation is that the spent flow with an inline configuration is channeled better than the 'slalom' flow between the jets in the staggered one.

In a review, Lee and Vafai [25] concluded that the effect of the spent flow can be neglected if

$$\frac{H}{d}\frac{w_c}{w} < 0.1 \tag{18}$$

where w is the jet velocity at the nozzle and w_c is the crossflow velocity.

It is possible to correlate w and w_c by calculating V_a, the flow rate from an array of jets in two ways. If we assume that the jet velocity is the same for all the nozzles (which depends on the jet flow manifold design, flow rate, and indeed the spent flow effect), since the number of jets by array is L/X, we have

$$V_a = \frac{L}{X}\frac{\pi d^2}{4} w \tag{19}$$

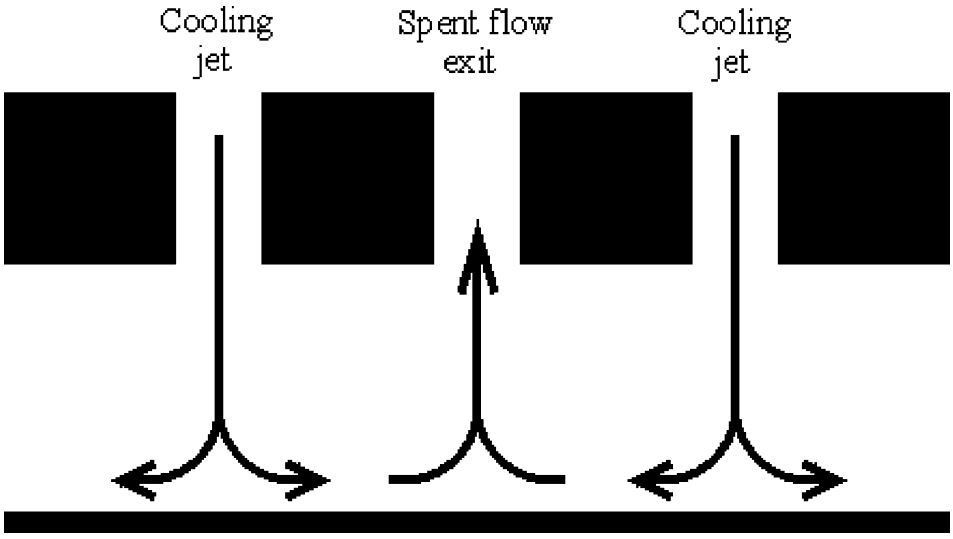

Fig. 14. Design to reduce the spent flow effects: intermediate holes suck out the spent air.

where X is the jet pitch in the direction of the crossflow and L the ring height. In the ideal case, the spent air would exit symmetrically toward both sides, and we get

$$V_a = 2YHw_c \tag{20}$$

where Y the jet pitch in the perpendicular direction. Then, combining (19) and (20), we obtain

$$w_c = \frac{L}{2X}\frac{\pi d^2}{4HY}w \tag{21}$$

Using this expression in Eq. (18) formulates the criterion as

$$\frac{L\pi d}{XY} < 0.8 \tag{22}$$

In the original design case studied here, the value of this factor is 3.5, indicating that the spent flow effect is not negligible. It is noteworthy that this criterion is independent of H.

As explained earlier, the spent flow has little effect in the symmetric axial mid-plane, but reduces the heat transfer coefficient at the ring edges. The main consequence of the spent flow is thus to create an axially nonuniform convective heat transfer coefficient, and hence a nonuniform temperature field in the ring during quenching. Also, since it reduces h at the edges, it reduces the average h and thus the cooling rate.

A relatively simple suggestion for an experimental evaluation of the effect of the spent flow in the nozzle-ring device is to quench rings that have a smaller height than the ones planned for the device, at different vertical positions in the device. It is expected that the spent flow effect would, for example, cause poorer quenching at the bottom and at the top of the device than at its mid-height.

To limit the spent flow momentum, the jet flow should impinge on the ring only, and not above and/or below it. The jets not impinging on the ring are not only uselessly consuming blower power, but they also carry with them quantities of gas that has to be removed, thus increasing the spent flow.

Appropriate design of the cooling device can reduce the spent flow momentum. One of the most efficient ways for that would be to have the spent flow exit parallel to the jets in the opposite direction, as shown in Fig. 14. This configuration would require a significantly different design than the original one but the spent flow virtually disappears. One of the simplest designs for that would be to use long tubes as nozzles, instead of holes through a plate. This would create a larger evacuation channel for the spent flow and thus reduce its momentum. This design is shown in Fig. 15a and b. Both figures represent the same nozzle arrangement (same t, d and

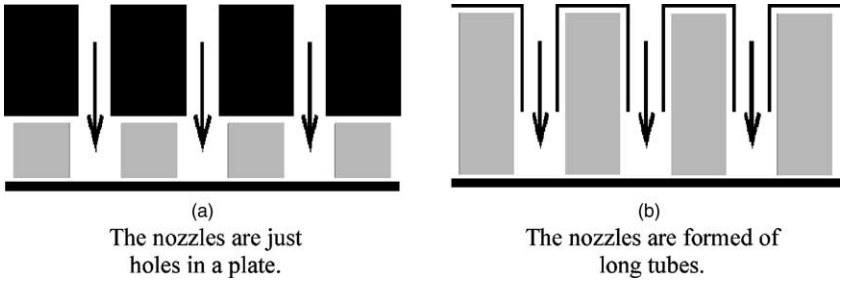

Fig. 15. A composition of the flow cross-section available for the spent air in the (a) existing design and (b) proposed improved design. The dark areas represent the plate, the solid material through which the holes are drilled. The gray areas represent roughly the available space available for the spent air to evacuate perpendicularly to the drawing plane. It can be seen that much more space is available for evacuating the spent air in configuration (b) than in (a).

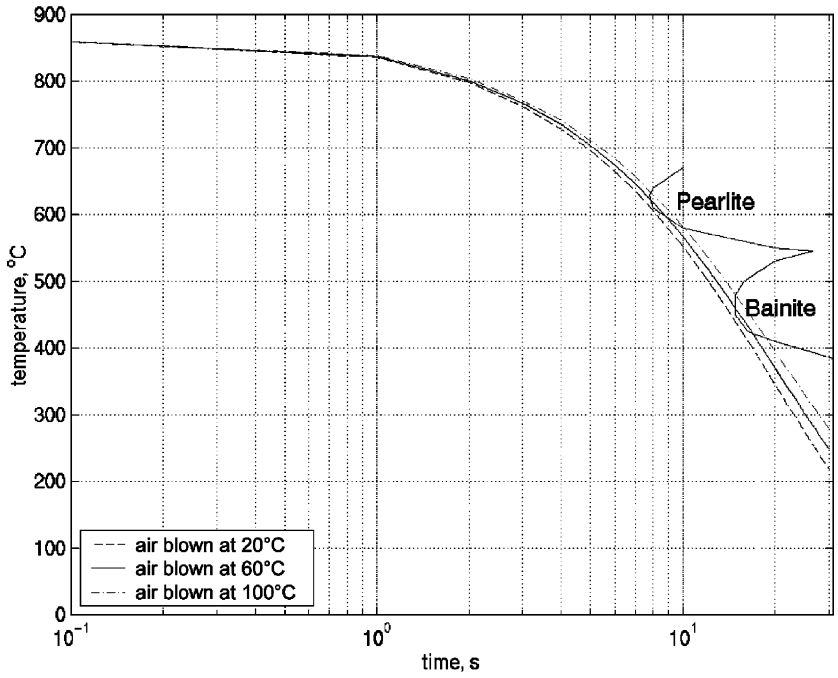

Fig. 16. Cooling curves of a 6.3 mm thick ring quenched by impinging air at different temperatures.

H), the gray rectangles represent the space between the jets available for the evacuation of the spent flow (perpendicularly to Fig. 15). It can be seen from Fig. 15 that this space is much larger where the nozzles are long tubes. The issue of spent flow effects requires further investigation.

7. Influence of the gas temperature

In this study it was assumed so far that the air impinging on the ring was at 20 °C, but it is known that the blower may heat the air to temperatures such as 60 or 80 °C. The effects of the gas temperature, T_g, are examined below.

It should be first noted that even if a higher gas temperature alters the cooling rates, the optimal nozzle arrangement, as described in Section 5, remains the same, since it is essentially independent of the gas temperature.

The analysis has shown that raising the cooling gas temperature from 20 to 100 °C increased, as expected, the velocity, but had an effect of less than 3% on h. It did, however, increase the power consumption at constant velocity (held close to the speed of sound, as the upper bound) by about 13%.

Since, as shown above, the effect of the gas temperature on h is negligible, only the temperature difference effect on the cooling rates is evaluated here. Fig. 16 shows the cooling curves of a 6.3 mm thick ring quenched by impinging air at different temperatures. All the curves show an identical pattern, the ring quenched with 20 °C gas is of course cooled faster than the one quenched with 100 °C gas. A cooling curve obtained for any gas temperature $T_{g,2}$ can be deduced from the cooling curve obtained with another gas temperature $T_{g,1}$ by using the equation

$$T(t)|_{T_{g,2}} = T_I - (T_I - T(t)|_{T_{g,1}}) \frac{T_I - T_{g,2}}{T_I - T_{g,1}} \quad (23)$$

8. Conclusions and recommendations

8.1. Conclusions

- Several formulas predicting the heat transfer coefficient for multiple impinging jets have been proposed. Martin's [5] formula is probably the most pertinent one. Gromoll's [14] formula predicts the highest convective heat transfer coefficients.
- The spent flow effect on h is not adequately known, but it tends to lower h.
- An optimal configuration of nozzles was recommended.
- Cooling curves for rings during quenching were computed by developing a numerical simulation of the transient heat conduction inside a ring. The resulting trends are very reasonable.
- The recommendations proposed in this report (and summarized below) for improvements of the nozzle-field quenching device, should indeed improve its quenching capability, but should be validated experimentally.

8.2. Recommendations for improving the nozzle-field quenching device

- The jet flows should impinge on the ring only and not above and/or below it to avoid useless power consumption and unnecessary spent flow disturbance.

- An inline arrangement of nozzle is preferred to a staggered one to diminish the detrimental effects of the evacuation of the spent flow.
- The nozzle array configuration proportions proposed in Section 5 should be observed, with the proportion $t = 1.324\,H$ being the most important. The proportion $d = 0.184\,H$ is also significant.
- While keeping these proportions, the three characteristic lengths H, t and d should be minimized.
- The spent flow effects should be investigated experimentally.
- If the spent flow proves to have an effect then the device should be redesigned, for example, by using long tubes as the jet nozzles (Section 6).

Acknowledgements

The sponsorship of this project by AGA AB, SKF Engineering and Research Center, B.V., and Volvo Personvagnar Komponenter AB, of this work at the Faxénlaboratoriet of the Kungl. Tekniska Högskolan (KTH), Stockholm, and the advice on metallurgical modeling from Dr. Anders Thuvander, the Swedish Institute for Metals Research, are gratefully acknowledged.

References

[1] S.J. Midea, T. Holm, S. Segerberg, J. Bodin, T. Thors, K. Swartström, High pressure gas quenching—technical and economic considerations, in: Proceedings of the Second International Conference on Quenching and the Control of Distortion, ASM International, 1996, p. 157.
[2] M. Lind, N. Lior, F. Alavyoon, F. Bark, Flows effects and modeling in gas-cooled quenching, in: Proceedings of the 11th International Conference on Heat Transfer, vol. 3, Korea, 1998, pp. 171–176.
[3] A. Thuvander, A. Melander, M. Lind, N. Lior, F. Bark, Prediction of convective heat transfer coefficients and their effects on distortion and mechanical properties of cylindrical tubes quenched by gas cooling, La Metallurgia Italiana, vol. XCI, no. 4, April 1999, pp. 25–32.
[4] J. Ferrari, N. Ipek, N. Lior, T. Holm, Flow considerations in quenching vessels, in: Proceedings of the Third ASM International Conference on Quenching and Control of Distortion, Czech Republic, Prague, 1999, pp. 93–101.
[5] H. Martin, Heat and mass transfer between impinging gas jets and solid surfaces, Adv. Heat Transf. 13 (1977) 1–60.
[6] R. Viskanta, Heat transfer to impinging isothermal gas and flame jets, Exp. Thermal Fluid Sci. 6 (1993) 111–114.
[7] FEMLAB, COMSOL AB, Tegnérgatan 23, Stockholm, Sweden. http://www.femlab.com/.
[8] MATLAB: The MathWorks, Inc., Natick, MA, USA. http://www.matlab.com/.
[9] J. Ferrari, Studies of flow and heat transfer in gas quench chambers, impingement cooled bodies, and inverse solutions, Licentiate Thesis, Technical Report 2002:02, ISSN 0348-467X, ISRN KTH/MEK/TR-02/02-SE, KTH, Stockholm, Faxénlaboratoriet, SE 100 44, Sweden, 2002.
[10] H.H. Ott, Wärmeübergang an einer durchLuft-strahlen gekühlten Platte, Schweiz. Bauzeitung 46 (1961) 834–840.
[11] H. Glaser, Untersuchungen an Schlitz- und Mehrdüsenanordnungen bei der Trocknung feuchter Oberflächen durch Warmluftstrahlen, Chemie-Ing. Techn. 3 (1962) 200–207.
[12] D.M. Kercher, W. Tabakoff, Heat transfer by a square array of round air jets impinging perpendicular to a flat surface including effect of spent air, Trans. ASME, J. Eng. Power 92 (1970) 73–82.
[13] R. Gardon, J. Cobonpue, Heat transfer between a flat plate and jets of air impinging on it, in: Proceedings of the Second ASME International Heat Transfer Conference, 1961–1962, University of Colorado, Boulder and London, UK, pp. 454–460.
[14] B. Gromoll, Experimentelle Untersuchungen des Wärmeübergangs an von Düsensystemen senkrecht angeströmten ebenen Flächen, Dissertation, University of Aachen, Germany, 1978.
[15] R. Kübler, Institute of Material Science and Engineering I, University of Karlsruhe, Germany, Personal communication, 2000.
[16] H.K.D.H. Bhadeshia, Bainite in Steels—Transformations, Microstructure and Properties, 2nd ed., Institute of Metals, IOM Communications Ltd., London, 2001. ISBN 1-86125-112-2.
[17] M. Avrami, Kinetics of phase change I, J. Chem. Phys. 7 (1939) 1103–1112.
[18] M. Avrami, Kinetics of phase change II, J. Chem. Phys. 8 (1940) 212–224.
[19] M. Avrami, Kinetics of phase change III, J. Chem. Phys. 9 (1941) 177–184.
[20] E.J. Mittemeijer, Analysis of kinetics of phase transformations, J. Mater. Sci. 27 (1992) 3977.
[21] E.B. Hawbolt, B. Chau, J.K. Brimacombe, Kinetics of austenite–pearlite transformation in eutectoide carbon steel, Metall. Trans. A 14 (1983) 1803–1815.
[22] S. Sjöström, The calculation of quench stresses in steel, Linköping Studies in Science and Technology, Dissertations, No. 84, University of Linköping, Sweden, 1982.
[23] A. Thuvander, Numerical simulation of distortion due to heat treatment, Licentiate Thesis, Report KTH/AMT-143, Royal Institute of Technology, Stockholm, Sweden, 1995.
[24] L.W. Florschuetz, C.R. Truman, D.E. Metzger, Streamwise flow and heat transfer distributions for jet array impingement with crossflow, J. Heat Transf. 103 (1981) 337–342.
[25] D.-Y. Lee, K. Vafai, Comparative analysis of jet impingement and microchannel cooling for high heat flux applications, Int. J. Heat Mass Transf. 42 (1999) 1555–1568.